PRAMANA
— journal of
physics

Vol. 86, No. 1
January 2016
pp. 31–48

Wave packet construction in three-dimensional quantum billiards: Visualizing the closed orbit, collapse and revival of wave packets in the cubical billiard

MANINDER KAUR[1,2,*], BINDIYA ARORA[1] and MAHMOOD MIAN[1]

[1]Department of Physics, Guru Nanak Dev University, Amritsar 143 005, India
[2]Department of Physics, D.A.V. College, Amritsar 143 005, India
*Corresponding author. E-mail: mannu_711@yahoo.co.in

MS received 14 February 2014; revised 21 October 2014; accepted 27 October 2014
DOI: 10.1007/s12043-015-0959-y; ***e*Publication:** 20 June 2015

Abstract. We examine the dynamical evolution of wave packets in a cubical billiard where three quantum numbers (n_x, n_y, n_z) determine its energy spectrum and consequently its dynamical behaviour. We have constructed the wave packet in the cubical billiard and have observed its time evolution for various closed orbits. The closed orbits are possible for certain specific values of quantum numbers (n_x, n_y, n_z) and initial momenta (k_x, k_y, k_z). We observe that a cubical billiard exhibits degenerate energy levels and the path lengths of the closed orbits for these degenerate energy levels are identical. In spite of the identical path lengths, the shapes of the closed orbits for degenerate levels are different and depend upon angles θ and ϕ which we term as the sweep and the elevation angles, respectively. These degenerate levels owe their origin to the symmetries prevailing in the cubical billiard and these levels disappear completely or partially for a parallelepiped billiard as the symmetry breaks due to commensurate or incommensurate ratio of sides.

Keywords. Three-dimensional bound systems; revivals and collapses; quantum mechanics.

PACS Nos 03.65.Ge; 03.65.Yz; 42.50.Md

1. Introduction

The study of time evolution of the unbound and bound-state wave packet illuminates many features of the wave mechanics. These include both semiclassical features as well as purely quantum mechanical effects. In the classical regime, the wave packet mimics a classical particle and in the quantum regime, the wave packet undergoes a sequence of collapses and revivals as a manifestation of the underlying quantum interference effects. The dynamics of the unbound and bound wave packets have been visualized by many researchers [1–9]. This approach of visualization of the dynamics of the wave packet has facilitated the understanding of highly nonclassical and the least intuitive quantum phenomenon. As a consequence, such visualizations have become increasingly relevant

as a pedagogical tool. The dynamical behaviour of the bound-state wave packets in the quantum systems where the energy spectrum depends on a single quantum number has been discussed in several studies [10–14]. In all these bound-state quantum systems, the dynamics of the wave packets (which are mostly the Gaussian wave packets (GWP)) lucidly reveal the existence of the phenomenon of collapses, revivals, fractional revivals and super-revivals of the wave packets. Moreover, the study of dynamics of the initial GWP trapped inside the bound potential wells can provide information about the shape and length of the closed orbits. For a system with only one degree of freedom, the closed orbits are simple to and fro trajectories with length equal to double the width of bounding potential. The system has been widely studied by a number of groups in two dimensions [15–18]. The motivation to extend the study to a three-dimensional (3D) system is the existence of real-world systems that cannot be reduced to 2D idealization and exhibit some (both classical and quantum) genuine 3D effects.

Billiards are widely being studied in the field of quantum chaos [19] and play an important role in extending this field to the system with more than two degrees of freedom [20–23]. They are also central to the investigation of 3D chaos in the resonant optical cavities [24]. In the theory of quantum chaos, connection between the chaotic behaviour of classical systems and specific properties of their quantum mechanical counterparts has received much attention [25–27]. One way to make this connection is to look at the eigenstate of billiards which exhibit a structure corresponding to the classical orbits [28]. These structures, called scars, have been directly related to unstable periodic orbits [29,30]. Visual inspection of movies that show the time evolution of probability distribution of a quantum particle moving in 2D and 3D billiards of different shapes strongly suggest that these sequence of images may contain enough information to distinguish between classical, integrable and chaotic systems [31]. The other important application of the theory of quantum billiards is related to the double-clad fibres. In such a fibre, a small core with low numerical aperture confines the signal and the wide cladding confines the multimode pump. In the paraxial approximation, the complex field of pump in the cladding behaves like a wave function in quantum billiard [32].

In this paper, we study the billiard problem in three dimensions. We have observed that in a cubical billiard, the degenerate energy levels belong to those set of quantum numbers (n_x, n_y, n_z) for which the expression $n_x^2 + n_y^2 + n_z^2 = D$ evaluates to an identical constant. Further, for a cubical billiard the path lengths of closed orbits are proportional to the quantity $\sqrt{n_x^2 + n_y^2 + n_z^2}$. Hence the lengths of the closed orbits for the degenerate energy levels are equal. We have observed that in spite of identical path lengths, the shapes of the closed orbits for these degenerate levels are different and depend upon two angles θ and ϕ which we term as the sweep angle and elevation angles, respectively.

To begin with, in §2, we discuss the basic properties of a GWP. Further we review the various time-scales viz., classical, revival and the super-revival time periods for a general one-dimensional (1D) bound system. In §3, we employ the general formulae of §2, to completely define the specific bound system of 1D infinite square well (ISW) centred at $x = 0$. In §4, we formulate the theoretical background for a cubical billiard. We discuss the general time dependence, condition for the closed orbits and the wave packet construction in the cubical billiard. Here we also define θ and ϕ. Also in this section, we discuss the degenerate states in the cubical billiard and the shapes of the closed orbits for the set of degenerate states. In §5, we provide a general overview of the results for a

parallelepiped billiard. In §6, we present our results for the dynamics of the GWP along various closed orbits in a cubical billiard and pattern of collapses and revivals of the GWP. The results are presented in the form of plots of position probability density at sequential instants of time within one classical time period and autocorrelation function for the short time (time $\sim$ few classical time periods) as well as the long time (time $\sim$ few revival time periods). We have also produced the animations which clearly illustrate the dynamics of the wave packet and shapes of the various closed orbits depending upon different initial conditions.

2. Gaussian wave packet

Consider a GWP described by the wave function

$$\psi(x,0) = \frac{1}{\sqrt{\sigma_0\sqrt{\pi}}}\exp(\iota k_0(x-x_0))\exp(-(x-x_0)^2/2\sigma_0^2). \tag{1}$$

This GWP is centred at $x = x_0$, with standard deviation, $\sigma_0/\sqrt{2}$. The corresponding momentum space wave function is

$$\psi(k,0) = \frac{1}{\sqrt{\sigma_0\sqrt{\pi}}}\exp(-\sigma_0^2(k-k_0)^2/2)\exp(-\iota(k-k_0)x_0). \tag{2}$$

This GWP is centred at $k = k_0$, with standard deviation $1/\sqrt{2}\sigma_0$. Here x_0 and k_0 correspond to initial position and initial momentum of the wave packet. The expectation value of the total kinetic energy is given by

$$\langle\hat{E}\rangle = \frac{1}{2m}\langle k^2\rangle\left(k_0^2 + \frac{1}{2\sigma_0^2}\right) \quad \text{with } \langle k^2\rangle = k_0^2 + 2\sigma_0^2.$$

If we expand such an initial GWP in terms of the energy eigenstates $U_n(x)$ of a general one-dimensional bound state potential [16], we have

$$\psi(x,0) = \sum_{n=1}^{\infty} a_n U_n(x), \tag{3}$$

where

$$a_n = \int_{-\infty}^{\infty} U_n^*(x)\psi(x,0)\mathrm{d}x. \tag{4}$$

The resulting a_n must satisfy the following two constraints:

$$\sum_{n=1}^{\infty}\left|a_n^2\right| = 1, \tag{5}$$

$$\sum_{n=1}^{\infty}\left|a_n^2\right| E_n = \langle\hat{E}\rangle, \tag{6}$$

where E_n represents the energy eigenvalues of the bound-state potential. The time dependence of the initial GWP as given by the solution of the time-dependent Schrödinger wave equation is

$$\psi(x,t) = \sum_{n=1}^{\infty} a_n U_n(x)\exp(-\iota E_n t/\hbar), \tag{7}$$

The coefficients a_n are defined by eq. (4). By taking the summation over n we restrict ourselves to the superposition to bound states only. This scenario appears when a GWP is trapped inside some potential well or a localized wave packet is produced experimentally using a short pulse laser [33,34]. Physically this localization is equivalent to the transformation of the GWP from the x-space to n-space via eq. (4). Thus, we shall end up with a GWP centred around the central value of the principle quantum number n_0 instead of a GWP centred around some position coordinate x_0. The mapping from the x-space to the n-space is brought about by the expansion coefficient a_n. Thus, it follows that the expansion is centred around a mean value n_0. If we expand the energy in a Taylor series around this mean value n_0, we get [15]

$$E_n \approx E_{n_0} + (n - n_0)E'_{n_0} + \frac{1}{2}(n - n_0)^2 E''_{n_0} + \frac{1}{6}(n - n_0)^3 E'''_{n_0} + \cdots, \tag{8}$$

where the primes over the energy terms represent derivatives of first-order, second-order, third-order and so on. These derivatives define the various time-scales depending upon the mean value n_0. The first time-scale

$$T_{\rm cl} = \frac{2\pi}{E'_{n_0}} \tag{9}$$

is the classical time period for the shortest closed orbit. It controls the initial behaviour of the wave packet. The second time-scale

$$T_{\rm rev} = \frac{2\pi}{\frac{1}{2}E''_{n_0}} \tag{10}$$

is the revival time. It governs the appearance of the fractional revivals and the full revivals. The third time-scale

$$T_{\rm sr} = \frac{2\pi}{\frac{1}{6}E'''_{n_0}} \tag{11}$$

is the super-revival time. It is larger than the classical and revival time periods.

The short-term and long-term behaviours of the wave packet are analysed using a standard tool popularly known as the autocorrelation function [35], given as

$$A(t) = \int_{-\infty}^{\infty} \psi^*(x,t)\psi(x,0)\mathrm{d}x \tag{12}$$

$$A(t) = \int_{-\infty}^{\infty} \phi^*(k,t)\phi(k,0)\mathrm{d}k \tag{13}$$

$$A(t) = \sum_n |a_n|^2 \exp(i E_n t/\hbar). \tag{14}$$

This measures the degree of overlap of the initial wave function with itself at later times.

3. One-dimensional infinite square well

We consider a 1D infinite square well centred at $x = 0$ and defined by

$$\begin{aligned} V(x) &= 0 \quad \text{for} \quad -1 < x < 1, \\ &= \infty \quad \text{for} \quad |x| > 1. \end{aligned}$$

The eigenfunction and eigenvalues of this quantum system are well defined and are given by (here $2m = \hbar = 1$),

$$U_n(x) = \sin(k_n(1+x)), \tag{15}$$

$$E_n = k_n^2, \tag{16}$$

$$k_n = \frac{n\pi}{L} = \frac{n\pi}{2}. \tag{17}$$

For a GWP defined by eq. (1) confined within this infinite square well, the expansion coefficient is evaluated using [16],

$$\begin{aligned} a_n &= \int_{-\infty}^{\infty} U_n^*(x)\psi(x,0)\mathrm{d}x, \\ &= \int_{-\infty}^{\infty} \sin(k_n(1+x))\psi(x,0)\mathrm{d}x, \\ &= \frac{1}{\sqrt{\sigma_0\sqrt{\pi}}} \int_{-\infty}^{\infty} \sin(k_n(1+x)) \exp(\iota k_0(x-x_0)) \\ &\quad \times \exp\left(-\frac{(x-x_0)^2}{2\sigma_0^2}\right)\mathrm{d}x. \end{aligned} \tag{18}$$

Using the standard integral

$$\int_{-\infty}^{\infty} \exp(-\alpha x^2 - bx)\mathrm{d}x = \sqrt{\frac{\pi}{\alpha}} \exp\left(\frac{\beta^2}{4\alpha}\right), \tag{19}$$

and

$$\sin(k_n(1+x)) = \frac{\exp(\iota k_n(1+x)) - \exp(-\iota k_n(1+x))}{2\iota}, \tag{20}$$

we obtain

$$a_n = \frac{\sqrt{2\sigma_0\sqrt{\pi}}}{2\iota}[\mathrm{e}^{\iota(k_n(1+x_0))}\mathrm{e}^{-(\sigma_0^2/8)(k_0+n\pi)^2} - \mathrm{e}^{-\iota(k_n(1+x_0))}\mathrm{e}^{-(\sigma_0^2/8)(k_0-n\pi)^2}]. \tag{21}$$

The closed orbits of the GWP in the 1D ISW are simple to and fro trajectories. The classical and revival time periods are given by

$$T_{\mathrm{cl}} = \frac{2\pi}{\left|E'_{n_0}\right|} = \frac{2\pi}{\pi^2 n_0/2} = \frac{4}{n_0\pi}, \tag{22}$$

$$T_{\mathrm{rev}} = \frac{2\pi}{\frac{1}{2}\left|E''_{n_0}\right|} = \frac{2\pi}{\pi^2/4} = \frac{8}{\pi}, \tag{23}$$

where E_n is defined by eq. (16).

4. Cubical billiard

For a cubical billiard, i.e., 3D ISW with dimensions $L_x \times L_y \times L_z = a \times a \times a$, the problem is equivalent to three 1D ISWs along the x, y and z directions and the eigenfunctions and eigenvalues are given as

$$w(x,y,z) = U_{n_x}(x)U_{n_y}(y)U_{n_z}(z), \tag{24}$$

$$E_{n_x,n_y,n_z} = k_{n_x}^2 + k_{n_y}^2 + k_{n_z}^2, \tag{25}$$

where n_x, n_y and n_z are appropriate quantum numbers and

$$k_{n_x} = \frac{n_x\pi}{L_x} = \frac{n_x\pi}{2},$$
$$k_{n_y} = \frac{n_y\pi}{L_y} = \frac{n_y\pi}{2},$$
$$k_{n_z} = \frac{n_z\pi}{L_z} = \frac{n_z\pi}{2},$$
$$U_{n_x}(x) = \sin(k_{n_x}(1+x)),$$
$$U_{n_y}(y) = \sin(k_{n_y}(1+y)),$$
$$U_{n_z}(z) = \sin(k_{n_z}(1+z)).$$

4.1 *Closed orbits*

Inside a cubical billiard the particle is free such that its total kinetic energy is constant implying that $v_x^2 + v_y^2 + v_z^2$ is fixed. In fact, the velocity components along the respective axis, i.e. v_x, v_y and v_z, are independently constant. The resultant magnitude and direction of these velocity components follows from the laws of vector addition. If v_n represents the resultant velocity and $k_n = mv_n$ represents the resultant momentum, the GWP proceeds along the resultant direction with net momentum k_n. This gives rise to a particular trajectory for a specific combination of v_x, v_y and v_z. With a change in any of the component velocity, the resultant trajectory alters. But all these possible trajectories do not result in a closed orbit. The closed orbits exist only if the following conditions are satisfied [16]:

$$\frac{k_{0y}}{k_{0x}} = \frac{n_y}{n_x}; \quad \frac{k_{0z}}{k_{0x}} = \frac{n_z}{n_x}; \quad \frac{k_{0z}}{k_{0y}} = \frac{n_z}{n_y}.$$

If p, q, r are numbers such that $2p, 2q, 2r$ give the number of hits on walls along the x, y, z directions, respectively, then in terms of these numbers the condition for the closed orbits is given by

$$n_x : n_y : n_z = p : q : r = \text{ a rational number.} \tag{26}$$

The length of the closed orbit $L(p, q, r)$ can be obtained from the simple geometrical construction [36] and is given by

$$L(p, q, r) = 2a\sqrt{p^2 + q^2 + r^2}. \tag{27}$$

The time period for the closed orbit is given by

$$T_{\text{cl}}^{(p_0)} = \frac{L(p, q, r)}{v_0} = \tau_{\text{cl}}\sqrt{p^2 + q^2 + r^2}, \tag{28}$$

$$\frac{T_{\text{cl}}^{(p_0)}}{\tau_{\text{cl}}} = \sqrt{p^2 + q^2 + r^2}. \tag{29}$$

Here v_0 is the classical speed and $\tau_{\text{cl}} = 2a/v_0$ is the classical time period for the simplest to and fro motion. Now,

$$T_{\text{rev}}^{(p_0)} = \frac{2\pi}{\frac{1}{2}|E_n''|}, \tag{30}$$

with $E_n = n^2\pi^2/L(p,q,r)$ which gives $E_n'' = 2\pi^2/L^2(p,q,r)$. Subsitituing for E_n'' with respect to revival time we get

$$T_{\text{rev}}^{(p_0)} = \frac{2}{\pi}L(p,q,r) = \frac{8}{\pi}a^2(p^2+q^2+r^2).$$

The above equation is simplified to a more useful form written as follows:

$$\frac{T_{\text{rev}}^{(p_0)}}{\tau_{\text{rev}}} = p^2+q^2+r^2, \tag{31}$$

where $\tau_{\text{rev}} = 8a^2/\pi$ is the revival time period for the shortest to and fro closed orbit.

Next, we calculate the values of n_x, n_y and n_z which lead to the closed orbits for the motion of wave function. The evaluation of the quantum numbers n_x, n_y and n_z is based on the total energy condition (eq. (25)), i.e.,

$$E(n_x,n_y,n_z) = \frac{1}{2}mv_n^2 = \frac{\pi^2}{4}\left(\frac{p^2+q^2+r^2}{p^2}\right)\times n_x^2. \tag{32}$$

From the above equation we get

$$n_x = \frac{v_n p}{\pi\sqrt{p^2+q^2+r^2}}. \tag{33}$$

Similarly,

$$n_y = \frac{v_n q}{\pi\sqrt{p^2+q^2+r^2}}, \tag{34}$$

$$n_z = \frac{v_n r}{\pi\sqrt{p^2+q^2+r^2}}. \tag{35}$$

From eq. (26) it follows that a particular closed orbit emerges for an appropriate choice of n_x, n_y and n_z. Consider a closed orbit as shown in figure 1. The construction of such a closed orbit requires that the sweep angle θ, elevation angle ϕ and the momentum components along the x, y, z axes be known. All these factors are defined in the following equations

$$\tan\theta = \frac{q}{p}, \tag{36}$$

$$\tan\phi = \frac{r}{\sqrt{p^2+q^2}}, \tag{37}$$

$$k_{0x} = k_0\frac{\sqrt{p^2+q^2}}{\sqrt{p^2+q^2+r^2}}\cos\theta, \tag{38}$$

$$k_{0y} = k_0\frac{\sqrt{p^2+q^2}}{\sqrt{p^2+q^2+r^2}}\sin\theta, \tag{39}$$

$$k_{0z} = k_0\sin\phi. \tag{40}$$

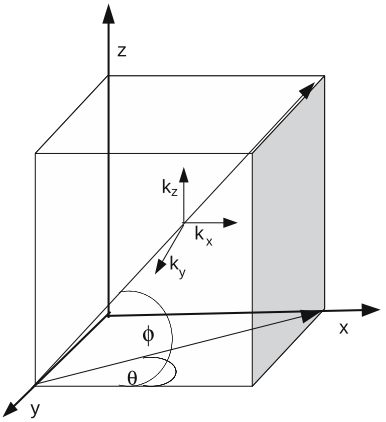

Figure 1. Closed trajectory in a cubical billiard. θ and ϕ are the sweep angle and the elevation angle. k_x, k_y and k_z are the momentum components along the x, y and z axes.

4.2 *Wave packet construction*

Time evolution of the initial GWP inside an ISW with three degrees of freedom is given by the following equation:

$$\phi(x, y, z) = \psi(x, t)\psi(y, t)\psi(z, t), \tag{41}$$

where

$$\psi(x,t) = \sum_{n_x=1}^{\infty} a_{n_x} U_{n_x}(x) \exp(-\iota E(n_x)t/\hbar),$$

$$\psi(y,t) = \sum_{n_y=1}^{\infty} a_{n_y} U_{n_y}(y) \exp(-\iota E(n_y)t/\hbar),$$

$$\psi(z,t) = \sum_{n_z=1}^{\infty} a_{n_z} U_{n_z}(z) \exp(-\iota E(n_z)t/\hbar).$$

Here,

$$a_{n_x} = \frac{\sqrt{2\sigma_0\sqrt{\pi}}}{2\iota}[\mathrm{e}^{\iota(k_{n_x}(1+x_0))}\mathrm{e}^{-(\sigma_0^2/8)(k_{0x}+n_x\pi)^2} - \mathrm{e}^{-\iota(k_{n_x}(1+x_0))}\mathrm{e}^{-(\sigma_0^2/8)(k_{0x}-n_x\pi)^2}],$$

$$a_{n_y} = \frac{\sqrt{2\sigma_0\sqrt{\pi}}}{2\iota}[\mathrm{e}^{\iota(k_{n_y}(1+y_0))}\mathrm{e}^{-(\sigma_0^2/8)(k_{0y}+n_y\pi)^2} - \mathrm{e}^{-\iota(k_{n_y}(1+y_0))}\mathrm{e}^{-(\sigma_0^2/8)(k_{0y}-n_y\pi)^2}]$$

and

$$a_{n_z} = \frac{\sqrt{2\sigma_0\sqrt{\pi}}}{2\iota}[\mathrm{e}^{\iota(k_{n_z}(1+z_0))}\mathrm{e}^{-(\sigma_0^2/8)(k_{0z}+n_z\pi)^2} - \mathrm{e}^{-\iota(k_{n_z}(1+z_0))}\mathrm{e}^{-(\sigma_0^2/8)(k_{0z}-n_z\pi)^2}]. \tag{42}$$

Table 1. Some of the possible values of the sweep angle θ, elevation angle ϕ, ratio of the classical time period and classical time period of the shortest closed orbit $T_{\rm cl}^{\rm po}/\tau_{\rm cl}$, ratio of revival time period and revival time period of the shortest closed orbit $T_{\rm rev}^{\rm po}/\tau_{\rm rev}$ and the degeneracy factor for the cubical billiard characterized by the integral values of p, q, r.

(p,q,r)	θ	ϕ	$T_{\rm cl}^{\rm po}/\tau_{\rm cl}$	$T_{\rm rev}^{\rm po}/\tau_{\rm rv}$	Degeneracy
(1,1,1)	45°	35.26°	$\sqrt{3}$	3	1
(1,1,2)	45°	54.74°	$\sqrt{6}$	6	
(1,2,1)	63.44°	24.09°	$\sqrt{6}$	6	3
(2,1,1)	26.57°	24.09°	$\sqrt{6}$	6	
(1,1,3)	45°	64.76°	$\sqrt{11}$	11	
(1,3,1)	71.57°	17.55°	$\sqrt{11}$	11	3
(3,1,1)	18.43°	17.55°	$\sqrt{11}$	11	
(1,2,3)	63.44°	53.30°	$\sqrt{14}$	14	
(3,1,2)	18.43°	32.31°	$\sqrt{14}$	14	
(2,3,1)	56.30°	15.50°	$\sqrt{14}$	14	6
(1,3,2)	71.57°	32.31°	$\sqrt{14}$	14	
(3,2,1)	33.69°	15.50°	$\sqrt{14}$	14	
(2,1,3)	26.57°	53.30°	$\sqrt{14}$	14	

4.3 *Degenerate states and closed orbits*

The association between the classical path length and the energy spectrum is well known, i.e., the Fourier transform of the density of quantized energy levels exhibits a delta function like peaks at distance values (L) corresponding to the length of closed orbits [36]. Thus, it is obvious that various degenerate energy levels will correspond to the identical path lengths of the closed orbits. However, the shapes of the closed orbits corresponding to degenerate energy levels depend upon the sweep angle θ and the elevation angle ϕ, which cannot be obtained from the Fourier analysis. Both these angles depend upon p, q, r or n_x, n_y, n_z and have been calculated in this work using eqs (36) and (37). Table 1 enlists some of the possible values of the sweep angle θ, elevation angle ϕ, time period of the corresponding closed orbit and the degeneracy factor for various combinations of integral values of p, q, r.

5. Parallelepiped billiard

Consider a parallelepiped billiard with sides $L_x \times L_y \times L_z = L \times 2L \times 4L$. For this case, the condition for closed orbits can be obtained from the fact that the classical close or periodic orbits are reproduced when the classical periods corresponding to the three quantum numbers n_x, n_y, n_z are commensurate [16], i.e.,

$$pT_{\rm cl}^{(n_x)} = qT_{\rm cl}^{(n_y)} = rT_{\rm cl}^{(n_z)} = T_{\rm cl}^{(\rm po)},$$

$$\frac{p}{\pi}\frac{L_x^2}{n_x} = \frac{q}{\pi}\frac{L_y^2}{n_y} = \frac{r}{\pi}\frac{L_z^2}{n_z},$$

$$\frac{pL_x}{n_x/L_x} = \frac{pL_y}{n_y/L_y} = \frac{pL_z}{n_z/L_z}. \tag{43}$$

Thus, the condition for the closed orbit is modified to

$$\frac{n_x}{L_x} : \frac{n_y}{L_y} : \frac{n_z}{L_z} = pL_x : qL_y : rL_z, \tag{44}$$

and the total energy condition becomes

$$E = \frac{1}{2}mv_0^2 = \pi^2 \left(\frac{n_x^2}{L_x^2} + \frac{n_y^2}{L_y^2} + \frac{n_z^2}{L_z^2} \right). \tag{45}$$

Equations (44) and (45) lead to

$$\begin{aligned}
\frac{n_x}{L_x} &= \frac{v_0}{2\pi} \left[\frac{pL_x}{\sqrt{(pL_x)^2 + (qL_y)^2 + (rL_z)^2}} \right], \\
\frac{n_y}{L_y} &= \frac{v_0}{2\pi} \left[\frac{qL_y}{\sqrt{(pL_x)^2 + (qL_y)^2 + (rL_z)^2}} \right], \\
\frac{n_z}{L_z} &= \frac{v_0}{2\pi} \left[\frac{rL_z}{\sqrt{(pL_x)^2 + (qL_y)^2 + (rL_z)^2}} \right].
\end{aligned} \tag{46}$$

The length of the closed orbit is given by

$$\begin{aligned}
L(pL_x, qL_y, rL_z) &= 2\sqrt{(pL_x)^2 + (qL_y)^2 + (rL_z)^2}, \\
&= 2\sqrt{(p_1)^2 + (q_1)^2 + (r_1)^2},
\end{aligned} \tag{47}$$

where $pL_x = p_1$, $qL_y = q_1$ and $rL_z = r_1$. For a parallelepiped billiard with sides $L_x \times L_y \times L_z = L \times 2L \times 4L$, the shortest closed orbit is along the x-axis. So we define the time period of the closed orbits with respect to the classical time period of the shortest to and fro trajectory along the x-axis. The classical time period of the shortest to and fro trajectory along this axis is defined as $\tau_x = 2L_x/v_{0x}$. From eqs (28) and (47), we can deduce

$$T_{\mathrm{cl}}^{(p_0)}(n_x) = \frac{2L(p,q,r)}{v_{0x}} = \frac{2\sqrt{(pL_x)^2 + (qL_y)^2 + (rL_z)^2}}{v_{0x}}. \tag{48}$$

As $L_x : L_y : L_z = 1 : 2 : 4$,

$$\begin{aligned}
T_{\mathrm{cl}}^{(p_0)}(n_x) &= \frac{2L_x\sqrt{p^2 + (2q)^2 + (4r)^2}}{v_{0x}}, \\
\frac{T_{\mathrm{cl}}^{(p_0)}(n_x)}{\tau_x} &= \sqrt{p^2 + (2q)^2 + (4r)^2}.
\end{aligned} \tag{49}$$

Also the expressions for $\tan(\theta)$ and $\tan(\phi)$ modify as follows:

$$\begin{aligned}
\tan(\theta) &= \frac{q_1}{p_1} = \frac{qL_x}{pL_y}, \\
\tan(\phi) &= \frac{r}{\sqrt{p_1^2 + q_1^2}} = \frac{rL_z}{\sqrt{(pL_x)^2 + (qL_y)^2}}
\end{aligned} \tag{50}$$

and the condition for the degeneracy modifies to

$$\left(\frac{n_x}{L_x}\right)^2+\left(\frac{n_y}{L_y}\right)^2+\left(\frac{n_z}{L_z}\right)^2=D, \tag{51}$$

where D is a constant. Table 2 enlists values of the sweep angle θ, elevation angle ϕ, time period of the corresponding closed orbit and the degeneracy factor for some of the possible combinations of integral values of p, q, r for the parallelepiped billiard.

Comparing tables 1 and 2, we observe that switching from the paradigm of the symmetrical billiards to that of the unsymmetrical billiards removes the degeneracy of the states to a partial extent. The symmetric quantum billiard possesses degenerate states which can be termed as sister states with the same path lengths of the closed orbits. The path lengths depend upon the energy eigenvalue via the sum of the squares of quantum numbers, i.e., $(n_x^2+n_y^2+n_z^2)$. But the shapes of the closed orbits depend upon how the total energy is distributed amongst the quantum numbers n_x, n_y, n_z, i.e., the weight of n_x, n_y, n_z. For $n_x > n_y > n_z$, the weight of n_x is the highest. So the highest proportion of the energy is associated with n_x. Thus, the momentum imparted along the x-axis is maximum. This results in more number of reflections from the x-axis. Mathematically, the momentum imparted along the various axes is defined by the angles θ and ϕ. Thus, the shapes of the closed orbits depend upon the angles θ and ϕ, which will be discussed in the following section.

6. Results and discussions

As cubical billiard is a 3D system, the visualization of the time evolution of the GWP inside it requires 4D plots which are not easily possible. We have translated these 4D

Table 2. Values of the sweep angle θ, elevation angle ϕ, ratio of classical time period and classical time period of the shortest closed orbit $T_{\rm cl}^{\rm po}/\tau_{\rm cl}$, ratio of revival time period and revival time period of the shortest closed orbit $T_{\rm rev}^{\rm po}/\tau_{\rm rev}$ and the degeneracy factor for some of the possible combinations of integral values of p, q, r for the parallelepiped billiard.

(p,q,r)	θ	ϕ	$T_{\rm cl}^{\rm po}/\tau_{\rm cl}$	$T_{\rm rev}^{\rm po}/\tau_{\rm rv}$	Degeneracy
(1,0,0)	0°	0∘	1	1	1
(0,1,0)	90°	0°	2	1	1
(0,0,1)	90°	90°	4	1	1
(1,1,1)	63.44°	60.79°	$\sqrt{21}$	21	1
(1,1,2)	63.44°	74.38°	$\sqrt{69}$	69	1
(1,2,1)	75.96°	44.13°	$\sqrt{33}$	33	1
(2,1,1)	45°	54.74°	$\sqrt{24}$	24	1
(3,1,1)	33.69°	47.97°	$\sqrt{29}$	29	1
(1,1,3)	63.43°	79.44°	$\sqrt{149}$	149	1
(1,3,1)	80.54°	33.33°	$\sqrt{53}$	53	1
(2,2,1)	63.43°	41.81°	$\sqrt{36}$	36	
(4,1,1)	26.57°	41.81°	$\sqrt{36}$	36	2
(2,3,1)	71.57°	32.31°	$\sqrt{56}$	56	
(6,1,1)	18.43°	32.31°	$\sqrt{56}$	56	2

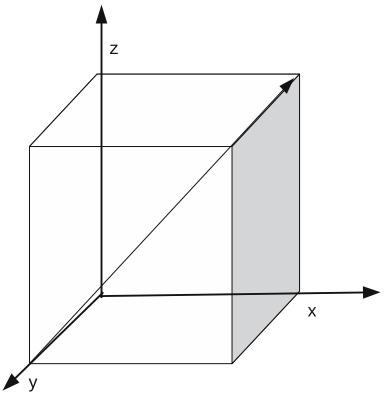

Figure 2. 3D view of the closed trajectory for $p = 1, q = 1, r = 1$.

plots to a grid in 3D. The plots are generated in MATLAB. The 3D view of the trajectory for these values are shown in figures 2, 3, 4 and 5. We have produced the plots of the probability density for (p, q, r) values (1, 1, 1) and (3, 1, 1), for a GWP centred at $n_0 = 500$. The trajectories for other (p, q, r) can be produced following the same procedure, but have not been presented in this work due to space constraint. It is important to select proper initial coordinates (x_0, y_0, z_0) in accordance with the slope that the trajectory will follow. The formulae to calculate these initial coordinates, for specific pair of angles θ and ϕ are given below. Here the value of x_0 is chosen independently and $|x| = |y| = |z| = 1$

$$\begin{aligned} |y_0| &= |y| - (|x| - |x_0|)\tan\theta, \\ |z_0'| &= \sqrt{(|x| - |x|_0)^2 + (|y| - |y|_0)^2}\tan\theta, \\ |z_0| &= |z| - |z_0'|. \end{aligned} \tag{52}$$

Figures 6 and 7 are the plots of the probability density showing the dynamics of the GWP in a cubical infinite square well for $p = 1, q = 1, r = 1$ at subsequent instants

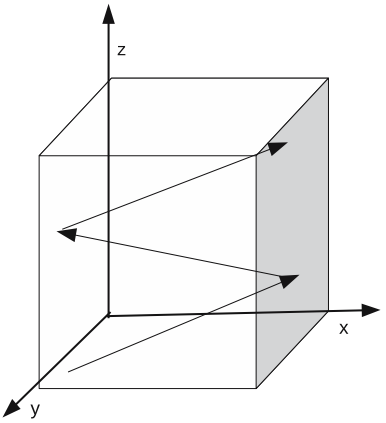

Figure 3. 3D view of the closed trajectory for $p = 3, q = 1, r = 1$.

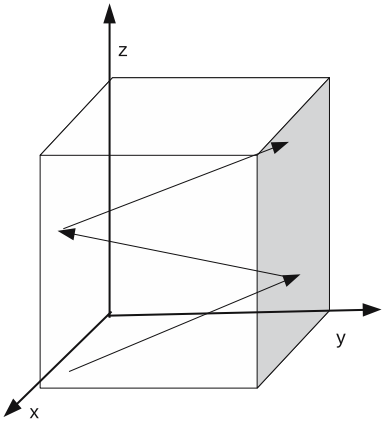

Figure 4. 3D view of the closed trajectory for $p = 1, q = 3, r = 1$.

of time. The classical time period of this trajectory is, $T_{\rm cl}^{\rm po} = \sqrt{3}(\approx 1.6) \times \tau_{\rm cl}$ which is endorsed by plot at $T_{\rm cl}^{\rm po} = 1.6 \times \tau_{\rm cl}$. Figure 6 shows the wave packet advancement along the diagonal of the cubical box from $T_{\rm cl}^{\rm po} = 0.1 \times \tau_{\rm cl}$ to $T_{\rm cl}^{\rm po} = 0.8 \times \tau_{\rm cl}$. Upto the time $T_{\rm cl}^{\rm po} = 0.4 \times \tau_{\rm cl}$, the GWP follows the classical path in forward direction. After this time, the wave packet collapses due to collision with the infinite potential walls. In figure 7 at about $T_{\rm cl}^{\rm po} = 1.3 \times \tau_{\rm cl}$, the wave packet revives and starts its backward journey along the same body diagonal.

Figures 8 and 9 are the plots of the probability density showing the dynamics of the GWP in the cubical billiard for one of the degenerate energy state (311) at subsequent instants of time. The classical time period $T_{\rm cl}^{\rm po} = \sqrt{11} \times \tau_{\rm cl}$.

Figure 10 shows the plots of the autocorrelation function, $|A(t)|^2$, vs. the ratio of classical time period and classical time period of the shortest closed orbit ($T_{\rm cl}^{\rm po}/\tau_{\rm cl}$) for all the nondegenerate pairs of (p, q, r), i.e., (1, 1, 1), (1, 1, 2), (1, 3, 1) and (1, 2, 3). The time spans from zero to twenty classical time periods. The plots confirm the $T_{\rm cl}^{\rm po}/\tau_{\rm cl}$

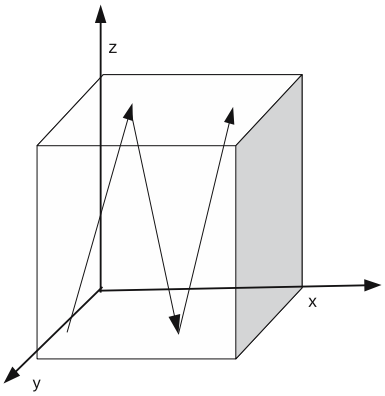

Figure 5. 3D view of the closed trajectory for $p = 1, q = 1, r = 3$.

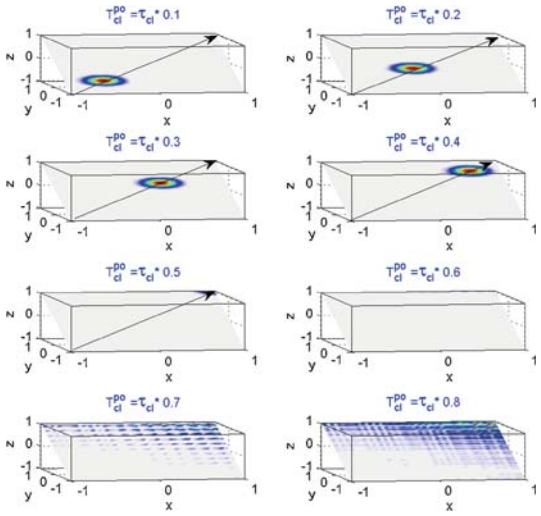

Figure 6. Closed trajectory for $p = 1, q = 1, r = 1$, forward motion of the GWP, the parameter $\sigma_0 = 0.25$. The initial points for the trajectory are $x_0 = -0.95$, $y_0 = -0.95$, $z_0 = -0.95$.

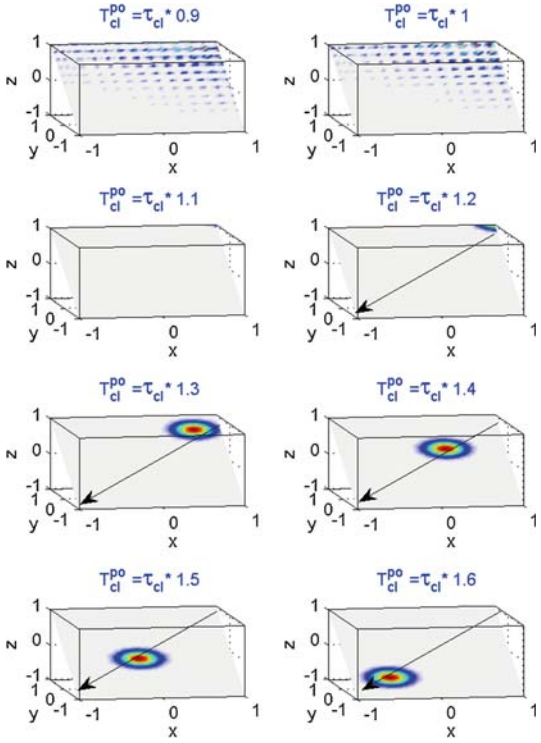

Figure 7. Closed trajectory for $p = 1, q = 1, r = 1$, backward motion of the GWP.

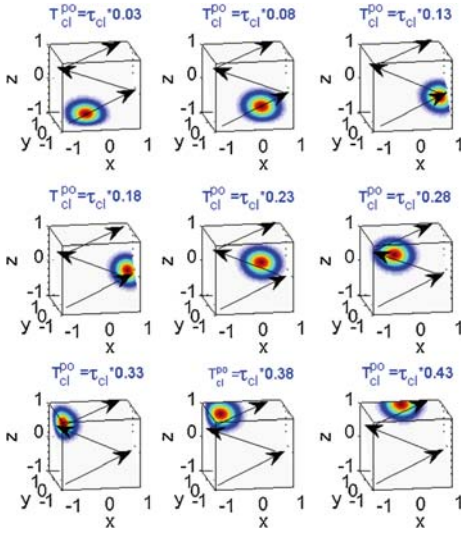

Figure 8. Closed trajectory for $p = 3, q = 1, r = 1$, forward motion of the GWP, parameter $\sigma_0 = 0.33$. The initial points for these trajectories are $x_0 = -0.7$, $y_0 = -0.9$, $z_0 = -0.68$.

values mentioned in table 1. The decreasing peak maxima validate the spreading of the wave packet for the successive rounds across the billiard.

Figure 11 plots the autocorrelation function, $|A(t)|^2$, vs. the ratio of revival time period and revival time period of the shortest closed orbit ($T^{\text{po}}_{\text{rev}}/\tau_{\text{rev}}$) for all the nondegenerate pairs of (p, q, r), i.e., (1, 1, 1), (1, 1, 2), (1, 3, 1) and (1, 2, 3). The time spans from zero to five revival time periods. The plots confirm the $T^{\text{po}}_{\text{rev}}/\tau_{\text{rev}}$ values mentioned in table 1.

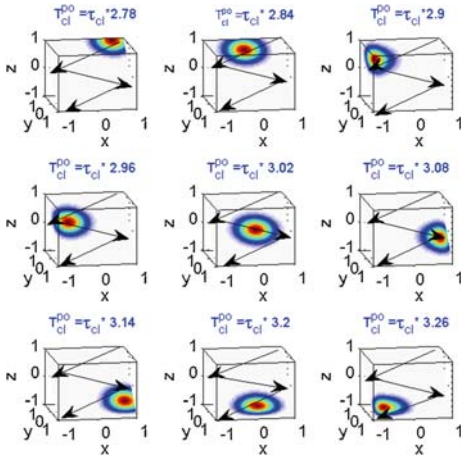

Figure 9. Closed trajectory for $p = 3, q = 1, r = 1$, backward motion of the GWP.

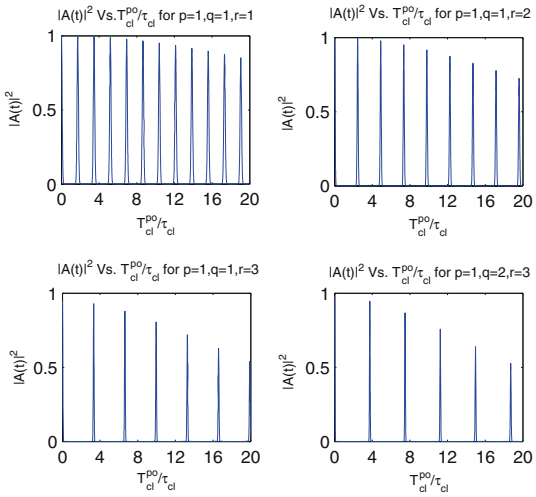

Figure 10. Plots of the autocorrelation function vs. the ratio of classical time period and classical time period of the shortest closed orbit, $T_{\rm cl}^{\rm po}/\tau_{\rm cl}$ for $(p, q, r) = (1,1,1)$, (1,1,2), (1,3,1) and (1,2,3) are $\sqrt{3}$, $\sqrt{6}$, $\sqrt{11}$ and $\sqrt{14}$, respectively. Parameter $\sigma_0 = 0.5$.

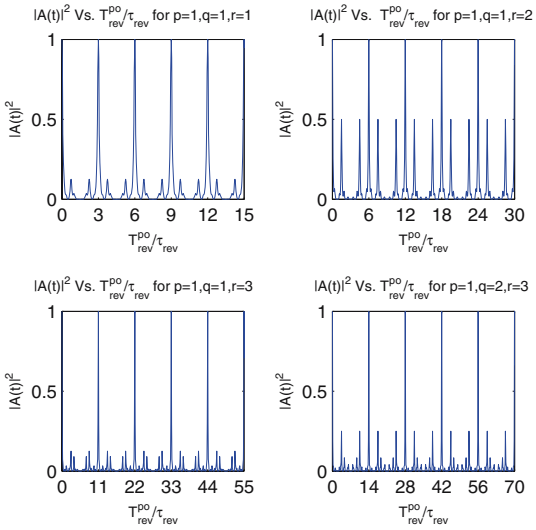

Figure 11. Plots of the autocorrelation function vs. the ratio of revival time period and revival time period of the shortest closed orbit, $T_{\rm rev}^{\rm po}/\tau_{\rm rev}$ for $(p, q, r) = (1,1,1)$, (1,1,2), (1,3,1) and (1,2,3) are 3, 6, 11 and 14, respectively. Parameter $\sigma_0 = 0.5$.

The constant peak maxima for the entire span of the revival time periods indicate the existence of an exact revival pattern in the cubical billiard. The smaller peaks show the presence of fractional revivals.

7. Scope of the work

Cubical and parallelepiped billiards are the potential candidates for the creation of artificial quantum confinement of electrons. These structures are termed as designer atoms or artificial atoms or quantum dots [37]. Designer atoms show the quantization of energy very similar to atoms. The advantage of designer atoms over natural atoms is that the number of confined electrons can be controlled. This paves the way to study many-electron interactions. It is difficult to study such interactions in natural atoms due to the presence of nucleus. Designer atoms also exhibit quantum mechanical behaviour such as shell structure and degeneracy [38], entanglement [39], tunnelling [40] and magnetization [41]. The shell structure of two-dimensional billiard with harmonic confining potential is studied in [37]. Our work can be extended to study the shell structure and shape of closed orbits in the case of three-dimensional infinite square well billiard with trapped electrons. Such studies are useful in low-dimensional condensed matter physics.

8. Conclusion

We have visualized the time evolution of the Gaussian wave packet bound inside the cubical billiard and have observed the various closed orbits. The length of the closed orbit depends upon the energy eigenvalue. Thus, the degenerate states of the cubical billiard belong to an identical path length. But the shapes of the closed orbits associated with these degenerate states are different as they depend upon the distribution of energy. The degeneracy originates due the symmetry of the cubical billiard. So, for a parallelepiped billiard, the degeneracy almost disappears except for a few degenerate states that depend upon the ratio of sides of the parallelepiped billiard.

Acknowledgement

The work of BA was supported by CSIR, grant number 03(1268)/13/EMR-II, India.

References

[1] A Goldberg, H M Schey and J L Schwartz, *Am. J. Phys.* **35**, 177 (1967)
[2] M H Bramhall and B M Casper, *Am. J. Phys.* **38**, 1136 (1970)
[3] M Andrews, *Am. J. Phys.* **66**, 252 (1998)
[4] C U Segre and J D Sullivan, *Am. J. Phys.* **44**, 729 (1976)
[5] A Edgar, *Am. J. Phys.* **63**, 136 (1995)
[6] L S Brown, *Am. J. Phys.* **41**, 525 (1973)
[7] Z D Gaeta and C R Stroud, *Phys. Rev. A* **42**, 6308 (1990)
[8] R Bluhm and V A Kostelecky, *Phys. Rev. A* **48**, R4047 (1993)
[9] R Bluhm and V A Kostelecky, *Phys. Rev. A* **49**, 4628 (1994)
[10] R Bluhm, V A Kostelecky and J A Porter, *Am. J. Phys.* **644**, 944 (1996)
[11] A Venugopalan and G S Agarwal, *Phys. Rev. A* **59(2)**, 1413 (1999)
[12] P Senn, *Am. J. Phys.* **60**, 228 (1992)
[13] R W Robinett, *Am. J. Phys.* **68**, 410 (2000)
[14] D L Aronstein and C R Stroud, *Phys. Rev. A* **55**, 4526 (1997)

[15] R W Robinett, *Phys. Rep.* **392**, 119 (2004)
[16] M A Doncheski, *Am. J. Phys.* **71**, 541 (2003)
[17] G S Agarwal and J Banerji, *Phys. Rev. A* **57**, 3880 (1998)
[18] R Bluhm, V A Kostelecky and B Tudose, *Phys. Lett. A* **222**, 220 (1996)
[19] T Guhr, A Müller-Groeling and H A Weidenmüller, *Phys. Rep.* **299**, 189 (1998)
[20] L Bunimovich, G Casati and I Guarneri, *Phys. Rev. Lett.* **77**, 2941 (1996)
[21] T Papenbrock and T Prosen, *Phys. Rev. Lett.* **84**, 262 (2000)
[22] H Primack and U Smilansky, *Phys. Rev. Lett.* **74**, 4831 (1995)
[23] T Prosen, *Phys. Lett. A* **233**, 323 (1997)
[24] J U Nöckel and A D Stone, *Nature* **385**, 45 (1997)
[25] S Blumberg and G E Porter, *Phys. Rev.* **110**, 786 (1958)
[26] M V Berry and M Tabor, *Proc. R. Soc. London Ser. A* **356**, 375 (1977)
[27] H Primack and U Smilansky, *Phys. Rep.* **327**, 1 (2000)
[28] E J Heller, *Phys. Rev. Lett.* **53**, 1515 (1984)
[29] E B Bogomolny, *Physica D* **31**, 169 (1988)
[30] M Feingold *et al*, *Phys. Lett. A* **146**, 199 (1990)
[31] J Kole, K Michielsen and H D Raedt, arXiv:nlin/0002055v3, 10 (2008)
[32] P Leproux, S Fevrier, V Doya, P Roy and D Pagnoux, *Opt. Fiber Technol.* **4**, 324 (2003)
[33] J Parker and C R Stroud, *Phys. Rev. Lett.* **56**, 716 (1986)
[34] G Alber, H Ritsch and P Zoller, *Phys. Rev. A* **34**, 1058 (1986)
[35] M Nauenberg, *J. Phys. B* **23**, 385 (1990)
[36] R W Robinett, *Am. J. Phys.* **65**, 1167 (1997)
[37] L L Eivind, *VMC calculations of two-dimensional quantum dots* (University of Oslo, 2010) URL: https://www.duo.uio.no/handle/10852/10993
[38] S Tarucha, D G Austing, T Honda, R J van der Hage and L P Kouwenhoven, *Phys. Rev. Lett.* **77**, 3613 (1996)
[39] S Weiss, M Thorwart and R Egger, *Europhys. Lett.* **76**, 905 (2006)
[40] W Lu, L P Z Ji, K W West and A J Rimberg, *Nature* **423**, 422 (2003)
[41] G Burkard, D Loss and D P DiVincenzo, *Phys. Rev. B* **59**, 2070 (1999)